A simple and sensitive $Ce(OH)CO_3/H_2O_2$/TMB reaction system for colorimetric determination of H_2O_2 and glucose

Xiang Zhang, Xueqing Bi, Weihua Di*, Weiping Qin*

State Key Laboratory on Integrated Optoelectronics, College of Electronic Science and Engineering, Jilin University, Changchun 130012, People's Republic of China.

* Corresponding authors: 2699 Qianjin Street, Changchun 130012, China. E-mail: whdi@jlu.edu.cn (W. Di); wpqin@jlu.edu.cn (W. Qin) Tel: 86-431-85168240-8325, Fax: 86-431-85168240-8325

ABSTRACT

The detection for H_2O_2 is essential in many areas, including life activity, medical diagnosis, industry and agriculture production and environmental monitoring, etc. This work developed a simple and sensitive two-step reaction system $Ce(OH)CO_3/H_2O_2$/TMB for H_2O_2 determination. Upon sequential addition of H_2O_2 and TMB to $Ce(OH)CO_3$ powders, a typical color reaction occurred quickly, producing a characteristic blue color in a slightly acidic aqueous solution. The underlying reaction mechanism was proposed based on the color reaction catalyzed by mimetic enzyme. The dependence of the color depth on H_2O_2 concentration enabled the colorimetric determination of H_2O_2. This reaction system responds linearly and quickly in a wide H_2O_2 concentration range of 0–80 μM, and achieves a detection limit of 0.3 μM H_2O_2 and a relative standard deviation lower than 5.1%. This H_2O_2 sensing system was modified to allow for the detection of glucose since H_2O_2 is one of the main products in the oxidation reaction of glucose catalyzed by oxidase enzymes. In addition to a wide linear response, a low detection limit and a high reproducibility, our present reaction system for glucose determination showed a highly specific response to glucose due to the specificity of glucose oxidase to glucose.

Keywords: H_2O_2 detection; Glucose detection; oxidase mimics; Color reaction; Colorimetric method

1. Introduction

Hydrogen peroxide (H_2O_2), one important representative of the group of reactive oxygen species (ROS), is now known to be acted as one of the signaling molecules in a wide range of signaling transduction processes, such as in normal cell functions or disease progressions.[1,2] H_2O_2 is also involved in chemical, pharma-ceutical, and environmental processes. Therefore, H_2O_2 determination has been required in many areas, including medical diagnosis, industry and agriculture production, environmental monitoring, etc.[3]

On the other hand, H_2O_2 is also the byproduct of many enzymatic reactions by a large number of oxidases, thus enabling quantitative assays of the activity of the enzyme as well as various enzyme substrates such as protein and carbohydrate in living organisms via a H_2O_2-mediated process.[4–6]

To date, various analytical techniques have been developed for the detection of H_2O_2, such as high performance liquid chromatography (HPLC) detection,[7] optical sensing,[8–12] colorimetric method,[13–17] electrochemical analysis,[18,19] etc. Owing to the advantages of simplicity, cheapness as well as the fact there is no requirement for any sophisticated instrumentation, colorimetric methods show great potential for portable and inexpensive daily life applications. [20]

Recently, enzyme mimetics have attracted great attention because they possess several advantages over natural enzyme such as low cost and high stability against denaturation and protease digestion. Meanwhile, the development of enzyme mimics has also opened a new way for colorimetric assay of analyte. In 2007, Fe_3O_4 magnetic nanoparticles were firstly discovered to exhibit an intrinsic peroxidase-like catalytic activity,[21] which was used to achieve the colorimetric determination for H_2O_2 and glucose via a color reaction of substrate.[13] Subsequently, various types of nanomaterials including metal oxide, carbon, and noble metal have been developed to possess unique enzyme-mimicking catalytic activities.[22–26]

In this work, a simple and sensitive two-step reaction system, $Ce(OH)CO_3/H_2O_2$/TMB, was developed for H_2O_2 detection. $Ce(OH)CO_3$ powders were prepared by a simple hydrothermal reaction. The addition of H_2O_2 solution to

$Ce(OH)CO_3$ powders, followed by the addition of TMB at a slightly acidic pH condition, caused a typical color reaction, producing a characteristic blue color in aqueous solution. The color depth of the solution depended on the H_2O_2 concentration, thus enabling the colorimetric determination of H_2O_2. This reaction system was modified to be also suitable for glucose detection via a H_2O_2-mediated process since H_2O_2 is one of the products of the glucose oxidation reaction under the catalysis of glucose oxidase.

2. Experimental

2.1. Chemicals

Analytical grade $Ce(NO_3)_3 \cdot 6H_2O$, $CO(NH_2)_2$ (urea), hydrogen peroxide (H_2O_2), citric acid and sodium citrate were obtained from Beijing Chemicals Reagents, China. Glucose, glucose oxidase (GOx), fructose, maltose, lactose, 4-(2-hydroxyethyl)-1-piperazineethanesulfonic acid (HEPES) and 3,3',5,5'-tetramethylbenzidine (TMB) were purchased from Sigma-Aldrich Co. (Shanghai, China). MiliQ water was used throughout. All other chemical reagents were of analytical reagent grade. The citrate buffer was prepared by mixing an approximate ratio of citric acid and sodium citrate solutions.

2.2. Preparation of $Ce(OH)CO_3 \cdot H_2O$

$Ce(OH)CO_3$ colloidal particles were prepared via a urea-based hydrothermal process according to the previous literatures.[27] In a typical reaction, 1 mmol of $Ce(NO_3)_3 \cdot 6H_2O$ and 20 mmol urea were dissolved in 50 mL of deionized water. The above solution was first homogenized under magnetic stirring at room temperature for 30 min, and then transferred into a 100 mL Teflon-lined autoclave and heated to 160 °C for 2 h. After the autoclave was cooled down to room temperature naturally, the obtained precipitates were collected by centrifugation and washed with deionized water and ethanol several times, and then dried in the air at 80 °C for 12 h.

2.3. H_2O_2 detection

In a typical process of H_2O_2 detection using $Ce(OH)CO_3/H_2O_2$/TMB system, 40 μL of H_2O_2 solution was added into the reaction tube containing 0.5 mg of $Ce(OH)CO_3$

powder, and reacted at room temperature for 4 min. Subsequently, 2 mL of citrate buffer solution (pH = 3.6) and 0.5 mg of TMB was sequentially added to the above mixed solution and incubated at room temperature for 5 min. The supernatant was immediately moved to 4 mL of quartz cuvette for UV-vis absorption measurement. To establish the relationship between the absorbance and H_2O_2 concentration, H_2O_2 concentration was changed from 10 to 80 μM, but other reaction conditions keep the same according to the above experiment procedure. It is known that the solution pH is a key parameter to influence the color reaction.[21] It is found in our experiments that the optimal pH was approximately 3.6 (Fig. S1, supplementary information). Therefore, the color reaction in this work was carried out at pH 3.6 citrate buffer solution.

2.4. Glucose detection

The glucose solution with the concentrations ranging from 10 to 160 μM was prepared and 3.2 mg of GOx was dissolved in 20 mL HEPES buffer solution (pH = 6.5). In a typical process of glucose detection, 40 μL of glucose solution and 100 μL of GOx solution were sequentially added into a 10 mL tube and incubated at 37°C for 5 min. Then, 0.5 mg of $Ce(OH)CO_3$ powder was added to the above solution and reacted for 4 min. Subsequently, 2 mL of citrate buffer solution (pH = 3.6) and 0.5 mg of TMB was sequentially added to the above mixed solution and incubated for 5 min. The supernatant was immediately moved to 4 mL of quartz cuvette for UV-vis absorption measurement.

2.5. Characterizations

The X-ray powder diffraction (XRD) data were collected on an X'Pert MPD Philips diffractometer (CuKα X-radiation at 40 kV and 50 mA) in the 2θ range from 10º to 70º with a scanning step of 0.02º. The transmission electron microscopy observations were carried out using a JEOL 2200FS microscope. Samples for TEM investigations were prepared by first dispersing the particles in ethanol under assistance of ultrasonification and then dropping 1 drop of the suspension on a copper TEM grid coated with a holey carbon film. Fourier transform infrared (FT-IR) spectra (Mattson 5000) of the samples were measured in the range of 4000-500 cm^{-1} in transmission mode. The pellets were

prepared by adding 0.8 mg of the sample powder to 80 mg of KBr. The powders were mixed homogeneously and compressed at a pressure of 10 KPa to form transparent pellets. X-ray photoelectron spectroscopy (XPS) analysis was performed using a PHI Quantera SXM (ULVAC-PHI) device operating at a pressure of 10^{-8} Torr. The photoelectron emission spectra were recorded using a monochromatic Al Kα source (100 W). The angle between the x-ray direction and the emitted electron direction was 45°. The UV-vis absorbance measurements were carried out by with a Schimadzu UV-2550 scanning spectrophotometer.

3. Results and discussion

3.1. Preparation and characterization of Ce(OH)CO₃

$Ce(OH)CO_3$ was prepared via a urea-based hydrothermal precipitation reaction (Experimental section), in which urea serves as a precipitation agent of metal cations due to self decomposition into the OH^- and CO_3^{2-} at elevated temperatures.[27-29] The urea-based reaction is a simple and general route for the preparation of lanthanide hydroxylcarbonate.[27] Fig. 1(a) shows the XRD pattern of the as-prepared product. All diffraction peaks were well indexed to $Ce(OH)CO_3$ phase and no impurity peaks were identified, indicating that the product is single-phased $Ce(OH)CO_3$.

The FT-IR measurement (Fig. 1(b)) provided further evidence for the successful preparation of $Ce(OH)CO_3$. In the FT-IR spectrum, a strong and broad absorption bands peaking at 3400 cm^{-1} and a shoulder located at 1645 cm^{-1} are the characteristic absorption of H_2O molecules and hydroxyl groups (OH^-).[30] The presence of carbonate anions in the molecular structure was confirmed by the appearance of absorption doublets in the region 1350–1600 cm^{-1} (ν_3 of CO_3^{2-}, peaking at ~1417 and 1504 cm^{-1}) and also by the occurrence of multiple absorptions ranging from 500 to 1000 cm^{-1} (ν_2 and ν_4 of CO_3^{2-}).[27,31]

Insert Fig. 1

3.2 Reaction mechanism

In our preliminary experiment, it is interesting to find that, the addition of H_2O_2 solution to $Ce(OH)CO_3$ powders, followed by the addition of TMB at a slightly acidic

pH condition, caused a typical color reaction, producing a characteristic blue color in aqueous solution. In comparison, such color reaction was not observed for the mixed solution of TMB and H_2O_2 in the absence of $Ce(OH)CO_3$ or for the mixed solution of TMB and $Ce(OH)CO_3$ in the absence of H_2O_2. This phenomenon excited our curiosity to explore the underlying reaction mechanism in the $Ce(OH)CO_3/H_2O_2$/TMB reaction system.

To this end, several control experiments were performed as follows. (i) 0.5 mg of TMB alone was added to (2 mL + 40 μL) citrate buffer solution. After 5 min, no color transformed. (ii) 40 μL of H_2O_2 (60 μM) was added to 2 mL citrate buffer solution, and subsequently 0.5 mg of TMB was added. After incubation for 5 min, the resulting solution shows almost no color transformation (Fig. 2(a)), indicating that $Ce(OH)CO_3$ is indispensable for creating such color transformation in TMB solution. (iii) 0.5 mg of $Ce(OH)CO_3$ was added to (2 mL + 40 μL) citrate buffer solution, and subsequently 0.5 mg of TMB was added. After incubation for 5 min, the resulting solution does not produce the color transformation (Fig. 2(b)), indicating that the presence of H_2O_2 is also necessary for such a color reaction. (iv) 40 μL of H_2O_2 solution (60 μM) was first added to 0.5 mg of $Ce(OH)CO_3$, and reacted for 4 min. Subsequently, 2 mL of citrate buffer solution and 0.5 mg of TMB were sequentially added. After incubation for 5 min, the resulting mixed solution produces a deep blue color (Fig. 2(c)). The above comparison results concluded that the color reaction of TMB solution can occur only at the coexistence of $Ce(OH)CO_3$ and H_2O_2.

Insert Fig. 2

Based on the above comparison experiments, we proposed the following reaction mechanism. Upon the addition of H_2O_2 to $Ce(OH)CO_3$ powders, the color of the powders produced an instantaneous transformation from white to yellow (Fig. 3(a)), which was caused by a change in the oxidation state from Ce^{3+} to Ce^{4+}.[32] Simultaneously, a number of bubbles appeared in this process (Fig. 3(b)). XPS measurement confirms the change of the oxidation state from Ce^{3+} to Ce^{4+} as the reaction between $Ce(OH)CO_3$ and H_2O_2 occurs. As shown in Fig. 3(c), four peaks

labeled U, U_1 , V and V_1 , characteristic of Ce(III), are clearly present for $Ce(OH)CO_3$, while six peaks labeled as U, U_2 , U_3, V, V_2 , and V_3 , characteristic of Ce(IV), are observed after the reaction with H_2O_2, indicating the oxidation of Ce(III) in the process of the reaction of $Ce(OH)CO_3$ with H_2O_2.[33,34] Indeed, H_2O_2 as an oxidizing agent is able to oxidize $Ce(OH)CO_3$ to generate a number of small sized CeO_2 particles and simultaneously produce the gases CO_2 and O_2, as described in the reaction equation (1).[35] The generation of CeO_2 was confirmed by XRD, TEM and UV-vis absorption measurements. In the XRD pattern (Fig. 4(a) and Fig. S2), the intensities of the diffraction peaks of $Ce(OH)CO_3$ were weakened gradually upon the addition of H_2O_2 and the newly appearing diffraction peaks were well indexed to the cubic phase of CeO_2.[36] The broad diffraction peaks indicated the small size of CeO_2 particles generated. The size of CeO_2 particles was evaluated using Scherrer Equation to be around 5 nm. Transmission electron microscopy (TEM) observations indicated that a large number of nanosized particles were grown *in situ* at the surface of the original $Ce(OH)CO_3$ particles via an interfacial reaction of $Ce(OH)CO_3$ and H_2O_2 (Fig. 4(b) and (c)). The mesopores are formed between these neighboring nanoparticles as a result of gases released during the reaction.[29,37] High-resolution TEM shows the presence of the crystalline nanoscaled CeO_2. The measured interplanar spacing of 0.312 nm corresponds well to the lattice spacing of the plane (111) of CeO_2 (Fig. 4(d)), in good agreement with XRD analysis. UV-vis absorption spectrum exhibited the characteristic absorption of CeO_2 located in the UV region (Fig. 4(e)).[38]

In the previous literature by Perez's research team in 2009, nanoceria has first been reported to possess an intrinsic oxidase-like activity at the acidic condition, as it can quickly catalyze the oxidization of a series of organic substrates without any oxidizing agent (e.g. hydrogen peroxide) to produce a characteristic color, *i.e.*, a color reaction.[39] Therefore, in our present work, the added H_2O_2 oxidizes $Ce(OH)CO_3$ to generate CeO_2, which behaves as a oxidase mimic to catalyze the oxidation of TMB, producing a characteristic blue color in aqueous solution.

$$Ce(OH)CO_3 + H_2O_2 \rightarrow CeO_2 + CO_2 + O_2 + H_2O \quad (1)$$

Insert Fig.3

Insert Fig. 4

3.3 H_2O_2 detection

On the basis of this reaction mechanism, we inferred that the extent of color reaction depends on the quantity of CeO_2 generated in the reaction of $Ce(OH)CO_3$ with H_2O_2, which is determined by H_2O_2 concentration as other reaction conditions keep constant. Therefore, the relationship between the absorbance of the solution and H_2O_2 concentration can enable the colorimetric determination of H_2O_2 in the $Ce(OH)CO_3/H_2O_2$/TMB system.

Fig. 5(a) shows the UV-vis absorption spectra of the solution after the reaction of $Ce(OH)CO_3$/TMB system with various concentrations of H_2O_2 in a constant time interval. All UV-vis absorption spectra exhibited two major absorbance peaks around 370 and 652 nm, which are characteristic of oxidized TMB,[40] indicating that H_2O_2 oxidizes $Ce(OH)CO_3$ powders to generate nano-CeO_2 that acts as catalyst for TMB oxidation. With an increase of H_2O_2 concentration, the absorbance of the solution increases gradually.

Indeed, the variation of color depth of the solution as a result of the change of H_2O_2 concentration added can be observed directly by the naked eye, as shown in the photographs taken for samples treated with various concentrations of H_2O_2 (Fig. 5(b)). The dependence of the absorbance on H_2O_2 concentration shows the feasibility of H_2O_2 determination by using $Ce(OH)CO_3/H_2O_2$/TMB reaction system. This provides a simple, low-cost and convenient colorimetric assay for H_2O_2.

For a clear comparison, the absorbance at 652 nm relative to H_2O_2 concentration was collected in Fig. 5(c). Clearly, the absorption intensity shows a good linear relationship against H_2O_2 concentration in the range of 0−80 μM with a correlation coefficient $R^2 = 0.992$, indicating a wide linear response for H_2O_2 sensing. By a linear fitting, the regression equation for H_2O_2 was $A = 0.01 + 1050[H_2O_2]$ (M), where A represents the absorbance of the resulting solution at a given H_2O_2 concentration added. The detection limit (LOD) was defined by the equation $LOD = (3\sigma/s)$ at the signal-to-noise of 3, where σ is the standard deviation of the blank signals (n = 11) and s

is the slope of the calibration curve. Based on this equation, the LOD for H_2O_2 was calculated to be 0.3 μM. The reproducibility of the proposed sensing system towards H_2O_2 was studied. The relative standard deviation (RSD) was 3.3% and 5.1% for the determination of 5 μM and 80 μM H_2O_2 for seven repeated measurements, respectively. This indicates high reproducibility and reliability of this reaction system for H_2O_2 determination.

Insert Fig. 5

3.4 Glucose detection

Since H_2O_2 is a main product of GOx catalyzed reaction of glucose (equation (2)), $Ce(OH)CO_3/H_2O_2$/TMB system is modified to allow the detection of glucose via a H_2O_2-mediated process. Many earlier studies have shown that the catalytic activity of enzyme-like nanomaterials is much higher in acidic solution (pH less than 4.0) than that in neutral and basic solutions.[13] But the enzyme activity of GOx for glucose oxidation would be denatured in acidic solution.[13] Therefore, the detection of glucose by using enzyme-like nanomaterials usually involves two-step analytical processes. First, GOx is used to catalyze the oxidation of glucose at the neutral pH condition, and then the produced H_2O_2 oxidizes $Ce(OH)CO_3$ to generate CeO_2 that acts as oxidase mimic for TMB oxidation at the acidic pH condition.

$$C_6H_{12}O_{6(\text{glucose})} + O_2 + H_2O \xrightarrow{\text{GOx}} C_6H_{12}O_{7(\text{gluconic acid})} + H_2O_2 \qquad (2)$$

Fig. 6(a) records the UV-vis absorption spectra of the solution after the addition of a given concentration of glucose and a fixed concentration of GOx to $Ce(OH)CO_3$ powders, followed by the addition of TMB in an acidic pH condition. Similar to $Ce(OH)CO_3/H_2O_2$/TMB system examined earlier, the UV-vis absorption spectra exhibits two major characteristic absorbance peaks at 370 and 652 nm attributed to oxidized TMB, indicating that the glucose oxidation reaction has occurred, in which the generated H_2O_2 has oxidized $Ce(OH)CO_3$ to CeO_2 as oxidase mimetics for TMB oxidation, creating a typical color reaction. With an increase of the glucose concentration, the absorbance increases gradually. The typical blue color reaction is clearly observed by the naked eyes and the variation of color depth with the glucose

concentration is also visual (Fig. 6(b)). Therefore, the $Ce(OH)CO_3/H_2O_2$/TMB system for H_2O_2 determination was modified to also allow the colorimetric assay for glucose.

Insert Fig. 6

For a clear comparison, the absorbance at 652 nm relative to glucose concentration was collected in Fig. 6(c). Clearly, the absorbance shows a good linear relationship against glucose concentration in the range of 0−140 μM with a correlation coefficient R^2 = 0.998, indicating a wide linear response toward glucose. By a linear fitting, the regression equation for glucose was A = 0.001 + 2200[glucose] (M), where A represents the absorbance of the solution after the reaction of GOx/$Ce(OH)CO_3$/TMB with a given glucose concentration added. The detection limit (LOD) for glucose was defined by the equation LOD = (3σ/s) at the signal-to-noise of 3, where σ is the standard deviation of the blank signals (n = 11) and s is the slope of the calibration curve. Based on this equation, the LOD for glucose was calculated to be 0.4 μM.

To highlight the advantages of our sensing material over the previously reported ones, we made a comparison for the sensing performances of the various types of glucose biosensors, as summarized on Table 1. Obviously, our proposed sensing method exhibits a wide linear response range and a low detection limit.

To verify whether our present reaction system for glucose detection could work correctly following this linear function, we randomly selected two concentration points of glucose (15 and 70 μM) from this linear plot to measure the absorbance corresponding to these two glucose concentrations. Results showed that the measured absorption values fitted well with this linear sensing function: the relative deviations of the absorbance for 15 and 70 μM glucose were 4.4% and 2.8%, respectively, indicating acceptable precision of this method.

The selectivity of sensing is extremely important for detecting the analyte accurately. To verify the sensing selectivity of glucose/GOx/$Ce(OH)CO_3$/TMB system toward glucose, several glucose analogues, such as lactose, maltose and fructose, were used for control experiments to check the influence of their additions (two concentration points: 30 and 60 μM) on the absorbance of the solution, as shown in Fig. 7. Results

show that the addition of these glucose analogues has almost no interference with the detection of glucose since their presence does not result in a significant variation of the absorbance, compared to the case of glucose. This indicates that our present reaction system has a high selectivity toward glucose sensing in the presence of GOx, which should be ascribed to the specificity of GOx to glucose in the catalytic reaction.

Insert Fig. 7

4. Conclusions

In this paper, a simple and sensitive reaction system has been developed for the detection of both H_2O_2 and glucose via a colorimetric method. This reaction system responds linearly to H_2O_2 and glucose in a wide analyte concentration range within several minutes. The limits of detection are 0.3 μM and 0.4 μM for H_2O_2 and glucose, respectively. The relative standard deviation for H_2O_2 and glucose detection is lower than 5.1%. Furthermore, our present reaction system for glucose determination shows a highly specific response. With the simplicity, rapid response, low detection limit, high reproducibility and selectivity of this method, our developed reaction system for detecting H_2O_2 and glucose might have promising applications in biological and environmental chemistry.

Acknowledgment

We acknowledge financial support from the National Science Foundation of China (Grant Nos. 61178073, 61222508).

References

[1] S. G. Rhee, H_2O_2, a necessary evil for cell signaling, Science 312 (2006) 1882–1883.

[2] C. X. Li, S. Q. Wang, Y. M. Huang, Q. Wen, L. Wang, Y. H. Kan, Photoluminescence properties of a novel cyclometalated iridium(III) complex with coumarin-boronate and its recognition of hydrogen peroxide, Dalton Trans. 43 (2014) 5595–5602.

[3] M. Baghayeri, E. Nazaradeh Zare, M. Mansour Lakouraj, A simple hydrogen peroxide biosensor

based on a novel electro-magnetic poly(p-phenylenediamine)@Fe_3O_4 nanocomposite Biosens. Bioelectron. 55 (2014) 259–265.

4 H. Wang, Y. Bu, W. Dai, K. Li, H. Wang, X. Zuo, Well-dispersed cobalt phthalocyanine nanorods on graphene for the electrochemical detection of hydrogen peroxide and glucose sensing, Sens. Actuator B: Chem. 216 (2015) 298–306.

[5] L. Shang, S.J. Dong, Design of fluorescent assays for cyanide and hydrogen peroxide based on the inner filter effect of metal nanoparticles, Anal. Chem. 21 (2009) 1465–1470.

[6] L. Shang, S.J. Dong, G.U. Nienhaus, Ultra-small fluorescent metal nanoclusters: synthesis and biological applications, Nano Today 6 (2011) 401–408.

[7] S. Wiesufer, A. Boddenberg, A. P. Ligon, G. Dallmann, W. V. Turner, S. Gab, An automated instrument for determining atmospheric H_2O_2 and organic hydroperoxides by stripping and HPLC, Environ. Sci. Pollut. R. 4 (2002) 41–47.

[8] C. Tagad, S. Dugasani, R. Aiyer, S. Park, A. Kulkani, S. Sabharwal, Green synthesis of silver nanoparticles and their application for the development of optical fiber based hydrogen peroxide sensor, Sens. Actuator B: Chem. 183 (2013) 144–149.

[9] C. J. Lv, W. H. Di, Z. H. Liu, K. Z. Zheng, W. P. Qin, Luminescent $CePO_4$:Tb colloids for H_2O_2 and glucose sensing, Analyst 139 (2014) 4547–4555.

[10] X. Y. Shan, L. J. Chai, J. J. Ma, Z. S. Qian, J. R. Chen, H. Feng, B-doped carbon quantum dots as a sensitive fluorescence probe for hydrogen peroxide and glucose detection, Analyst 139 (2014) 2322–2325.

[11] H. Tan, C. Ma, Q. Li, L. Wang, F. Xu, S. Chen, Y. Song, Functionalized lanthanide coordination polymer nanoparticles for selective sensing of hydrogen peroxide in biological fluids, Analyst 139 (2014) 5516–5522.

[12] D. Sodzel, V. Khranovskyy, V. Beni, A. P. F. Turner, R. Viter, M. O. Eriksson, P. Holtz, J. Janot, M. Bechelany, S. Balme, V. Smyntyna, E. Kolesneva, L. Dubovakaya, I. Volotovski, A. Ubelis, R. Yakimova, Continuous sensing of hydrogen peroxide and glucose via quenching of the UV and visible luminescence of ZnO nanoparticles, Microchim Acta 182 (2015) 1819–1826.

[13] H. Wei, E. Wang, Fe_3O_4 magnetic nanoparticles as peroxidase mimetics and their applications in H_2O_2 and glucose detection, Anal. Chem. 80 (2008) 2250–2254.

[14] X. Chen, B. Su, Z. Cai, X. Chen, M. Oyama, PtPd nanodendrites supported on graphene

nanosheets: A peroxidase-like catalyst for colorimetric detection of H_2O_2, Sens. Actuator B: Chem. 201 (2014) 286–292.

[15] Z. C. Xing, J. Q. Tian, A. M. Asiri, A. H. Qusti, A. O. Al–Youbi, X. P. Sun, Two-dimensional hybrid mesoporous Fe_2O_3-graphene nanostructures: A highly active and reusable peroxidase mimetic toward rapid, highly sensitive optical detection of glucose, Biosens. Bioelectron. 52 (2014) 452–457.

[16] J. Q. Tian, Q. Liu, A. M. Asiri, A. H. Qusti, A. O. Al–Youbi, X. P. Sun, Ultrathin graphitic carbon nitride nanosheets: a novel peroxidase mimetic, Fe doping-mediated catalytic performance enhancement and application to rapid, highly sensitive optical detection of glucose, Nanoscale 5 (2013) 11604–11609.

[17] Y. W. Zhang, J. Q. Tian, S. Liu, L. Wang, X. Y. Qin, W. B. Lu, G. H. Chang, Y. L. Luo, A. M. Asiri, A. O. Al–Youbi, X. P. Sun, Novel application of CoFe layered double hydroxide nanoplates for colorimetric detection of H_2O_2 and glucose, Analyst 137 (2012) 1325–1328.

[18] S. Azizi, S. Ghasemi, A. Samadi-Maybodi, M. Ranjbar, A new modified electrode based on Ag-doped mesoporous SBA-16 nanoparticles as non-enzymatic sensor for hydrogen peroxide, Sens. Actuator B: Chem. 216 (2015) 271–278.

[19] M. Mahmoudian, Y. Alias, W. Basirun, P. Woi, M. Sookhakian, Facile preparation of MnO_2 nanotubes/reduced graphene oxide nanocomposite for electrochemical sensing of hydrogen peroxide, Sens. Actuator B: Chem. 201 (2014) 526–534.

[20] T. Lin, L. Zhong, Z. Song, L. Guo, H. Wu, Q. Guo, Y. Chen, F. Fu, G. Chen, Visual detection of blood glucose based on peroxidase-like activity of WS_2 nanosheets, Biosens. Bioelectron. 62 (2014) 302–307.

[21] L. Gao, J. Zhuang, L. Nie, J. Zhang, Y. Zhang, N. Gu, T. H. Wang, J. Feng, D. L. Yang, S. Perrett, Intrinsic peroxidase-like activity of ferromagnetic nanoparticles, Nat. Nanotechnol. 2 (2007) 577–583.

[22] Y. H. Lin, Z. H. Li, Z. W. Chen, J. S. Ren, X. G. Qu, Mesoporous silica-encapsulated gold nanoparticles as artificial enzymes for self-activated cascade catalysis, Biomaterials 34 (2013) 2600–2610.

[23] R. Zhang, S. He, C. Zhang, W. Chen, Three-dimensional Fe- and N-incorporated carbon structures as peroxidase mimics for fluorescence detection of hydrogen peroxide and glucose, J. Mater. Chem. B 3 (2015) 4146–4154.

[24] H. Wang, S. Li, Y. M. Si, Z. Z. Sun, S. Y. Li, Y. H. Lin, Recyclable enzyme mimic of cubic Fe_3O_4 nanoparticles loaded on graphene oxide-dispersed carbon nanotubes with enhanced peroxidase-like catalysis and electrocatalysis, J. Mater. Chem. B 2 (2014) 4442–4448.

[25] G. L. Wang, X. F. Xu, X. M. Wu, G. X. Cao, Y. M. Dong, Z. J. Li, Visible-light-stimulated enzymelike activity of graphene oxide and its application for facile glucose sensing, J. Phys. Chem. C 118 (2014) 28109–28117.

[26] S. Kumari, B. B. Dhar, C. Panda, A. Meena, S. Sen Gupta, Fe-TAML Encapsulated Inside Mesoporous Silica Nanoparticles as Peroxidase Mimic: Femtomolar Protein Detection, ACS Appl. Mater. Interfaces (6) 2014 13866 –13873.

[27] E. Matijevic，W. P. Hsu, Preparation and properties of monodispersed colloidal particles of lanthanide compounds: I. Gadolinium, europium, terbium, samarium, and cerium(III), J. Colloid Interface Sci. 118 (1987) 506–523.

[28] A. M. Kaczmarek, K. Van Hecke, R. Van Deun, Nano- and micro-sized rare-earth carbonates and their use as precursors and sacrificial templates for the synthesis of new innovative materials, Chem. Soc. Rev. 44 (2015) 2032–2059.

[29] W. Di, X. Ren, H. Zhao, N. Shirahata, Y. Sakka, W. Qin, Single-phased luminescent mesoporous nanoparticles for simultaneous cell imaging and anticancer drug delivery, Biomaterials 32 (2011) 7226–7233.

[30] L.Moscardini D'Assunção, I. Giolito, M. Ionashiro, Thermal decomposition of the hydrated basic carbonates of lanthanides and yttrium, Thermochim. Acta 137 (1989) 319–330.

[31] K. Makamoto, Infrared spectra of inorganic and coordination compounds. New York: John Wiley & Sons; 1963.

[32] L. W. Qian, X. Wang, H. G. Zheng, Controlled synthesis of three-fold dendrites of $Ce(OH)CO_3$ with multilayer caltrop and their thermal conversion to CeO_2, Cryst. Growth Des. 12 (2012) 271–280.

[33] G. Chen, F. Rosei, D. Ma, Interfacial reaction-directed synthesis of Ce–Mn binary oxide nanotubes and their applications in CO oxidation and water treatment, Adv. Mater., 22 (2012) 3914–3920.

[34] F. Zhu, G. Chen, S. Sun, X. Sun, *In situ* growth of Au@CeO2 core–shell nanoparticles and CeO_2 nanotubes from $Ce(OH)CO_3$ nanorods, J. Mater. Chem. A, 1 (2013) 288–294.

[35] F. H. Scholes, A. E. Hughes, S. G. Hardin, P. Lynch, P. R. Miller, Influence of hydrogen peroxide in the preparation of nanocrystalline ceria, Chem. Mater. 19 (2007) 2321–2328.

[36] S. Singh, T. Dosani, A. S. Karakoti, A. Kumar, S. Seal, W. T. Self, A phosphate-dependent shift in redox state of cerium oxide nanoparticles and its effects on catalytic properties, Biomaterials 32 (2011) 6745–6753.

[37] C. Yu, L. Zhang, J. Shi, J. Zhao, J. Gao, D. Yan, A simple template-free strategy to synthesize nanoporous manganese and nickel oxides with narrow pore size distribution, and their electrochemical properties, Adv. Funct. Mater. 18 (2008) 1544–1554.

[38] Y. Lin, C. Xu, J. Ren, X. Qu, Using Thermally regenerable cerium oxide nanoparticles in biocomputing to perform label-free, resettable, and colorimetric logic operations, Angew. Chem. Int. Ed. 51 (2012) 12579–12583.

[39] A. Asati, S. Santra, C. Kaittanis, S. Nath, J. Manuel Perez, Oxidase-like activity of polymer-coated cerium oxide nanoparticles, Angew. Chem. Int. Ed. 48 (2009) 2308–2312.

[40] Z. M. Tian, J. Li, Z. Y. Zhang, W. Gao, X. Zhou, Y. Qu, Highly sensitive and robust peroxidase-like activity of porous nanorods of ceria and their application for breast cancer detection, Biomaterials 59 (2015) 116–124.

[41] H. Zhang, X. Xu, Y. Yin, P. Wu, C. Cai, Nonenzymatic electrochemical detection of glucose based on Pd1Pt3-graphene nanomaterials, J. Electroanal. Chem. 690 (2013) 19–24.

[42] Y. Li, Y. Zhong, Y. Zhang, W. Weng, S. Li, Carbon quantum dots/octahedral Cu_2O nanocomposites for non-enzymatic glucose and hydrogen peroxide amperometric sensor, Sens. Actuator B: Chem. 205 (2015) 735–743.

[43] H. Wang, Y. Bu, W. Dai, K. Li, H. Wang, X. Zuo, Well-dispersed cobalt phthalocyanine nanorods on graphene for the electrochemical detection of hydrogen peroxide and glucose sensing, Sens. Actuator B: Chem. 216 (2015) 298–306.

[44] K. Wannajuk, M. Jamkatoke, T. Tuntulani, B. Tomapatanaget, Highly specific-glucose fluorescence sensing based on boronic anthraquinone derivatives via the GOx enzymatic reaction, Tetrahedron 68 (2012) 8899–8904.

[45] A. Dutta, S. Maji, A. Mondal, B. Karmakar, P. Biswas, B. Adhikary, Iron selenide thin film: Peroxidase-like behavior, glucose detection and amperometric sensing of hydrogen peroxide, Sens. Actuator B: Chem. 173 (2012) 724–731.

[46] Q. Li, G. Tang, X. Xiong, Y. Cao, L. Chen, F. Xu, H. Tan, Carbon coated magnetite nanoparticles with improved water-dispersion and peroxidase-like activity for colorimetric sensing of glucose, Sens. Actuator B: Chem. 215 (2015) 86–92.

[47] Y. Song, K. Qu, C. Zhao, J. Ren, X. Qu, Graphene Oxide: Intrinsic peroxidase catalytic activity and its application to glucose detection, Adv. Mater., 22 (2010) 2206–2210.

Figure captions

Fig. 1. XRD (a) and FT-IR spectrum (b) of the product prepared via the precipitation reaction of cerium nitrate and urea.

Fig. 2. (a) 0.5 mg of $Ce(OH)CO_3$ and 0.5 mg of TMB were sequentially added to (2 mL + 40 μL) citrate buffer solution; (b) 40 μL of H_2O_2 (60 μM) and 0.5 mg of TMB were sequentially added to 2 mL citrate buffer solution; (c) 40 μL of H_2O_2 solution (60 μM) was first added to 0.5 mg of $Ce(OH)CO_3$, and reacted at room temperature for 4 min. Subsequently, 2 mL of citrate buffer solution and 0.5 mg of TMB were sequentially added.

Fig. 3. Upon the addition of H_2O_2, the white color $Ce(OH)CO_3$ powders were changed to the yellow one (a); meanwhile, a number of bubbles appeared in this reaction due to the production of CO_2 and O_2 (b).

Fig. 4. XRD pattern, TEM image and UV-vis absorbance spectrum of the product obtained after the reaction of $Ce(OH)CO_3$ with H_2O_2 at room temperature.

Fig. 5. (a) The UV-vis absorption spectra of the solution after the reaction of $Ce(OH)CO_3$/TMB system with various concentrations of H_2O_2. (b) The corresponding photographs of the reaction solutions with the addition of different concentrations of H_2O_2 ranging from 10 to 80 μM. (b) The absorbance monitored at 652 nm as a function of H_2O_2 concentration.

Fig. 5. (a) The UV-vis absorption spectra of the solution after the reaction of $Ce(OH)CO_3$/TMB system with various concentrations of H_2O_2. (b) The corresponding photographs of the reaction solutions with the addition of different concentrations of H_2O_2 ranging from 10 to 80 μM. (b) The absorbance monitored at 652 nm as a function of H_2O_2 concentration.

Fig. 6. (a) The UV-vis absorption spectra of the solution after reaction of $Ce(OH)CO_3$/TMB system with various concentrations of glucose in the presence of GOx. (b) The corresponding photographs of the solution after the reaction with the addition of different concentrations of glucose ranging from 10 to 180 μM (from right to left). (c) The absorbance monitored at 652 nm as a function of glucose concentration.

Fig. 7. The absorbance of the solution in the reaction system GOx/$CeOHCO_3$/TMB with the addition of glucose or its analogues such as lactose, fructose and maltose, respectively. The error bars represent the standard deviation obtained by seven repeated experiments.

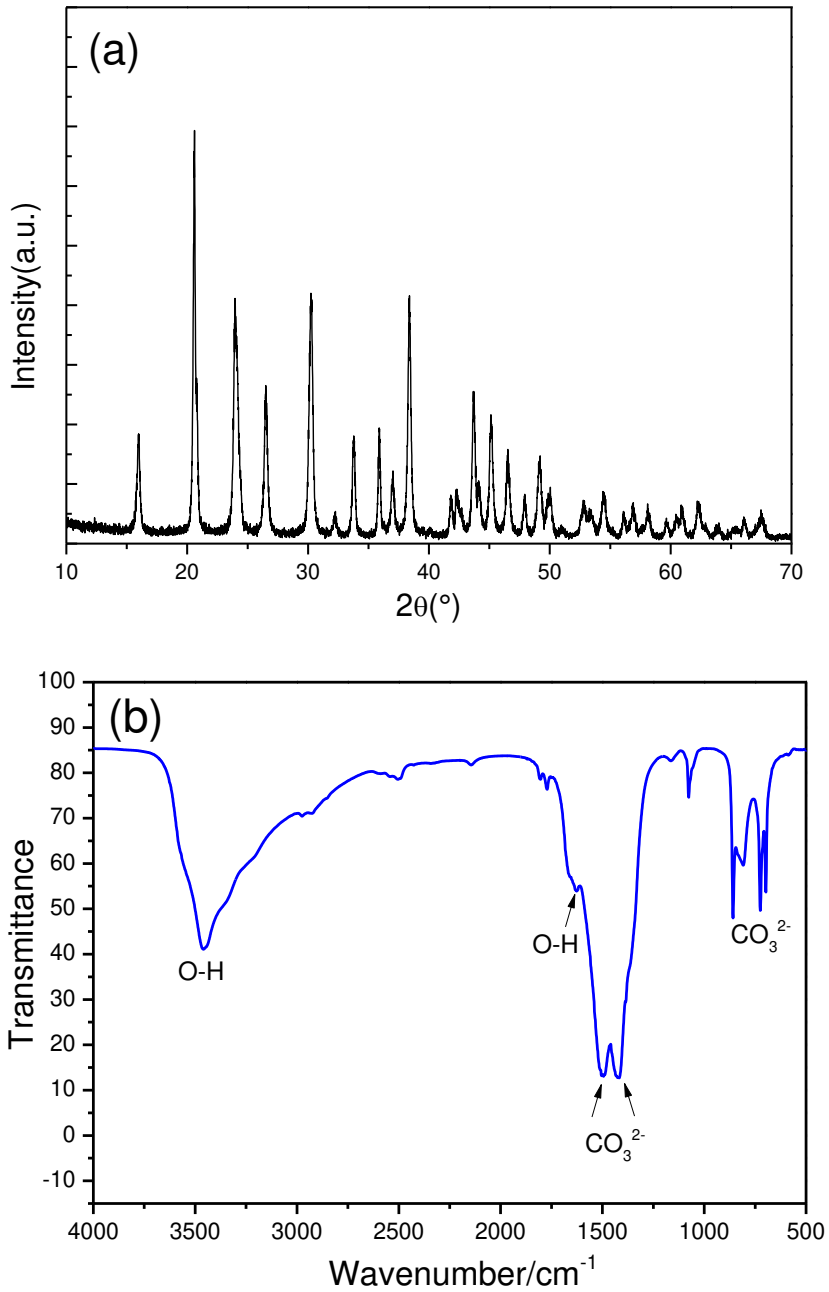

Fig. 1. XRD (a) and FT-IR spectrum (b) of the product prepared via the precipitation reaction of cerium nitrate and urea.

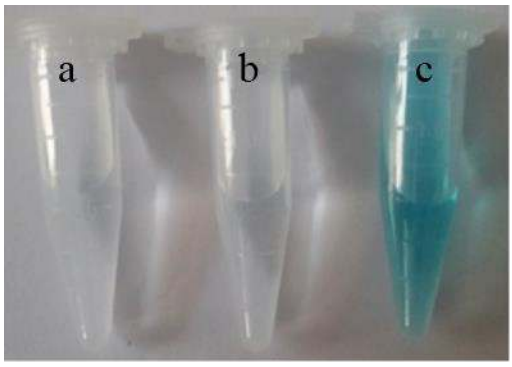

Fig. 2. (a) 0.5 mg of $Ce(OH)CO_3$ and 0.5 mg of TMB were sequentially added to (2 mL + 40 μL) citrate buffer solution; (b) 40 μL of H_2O_2 (60 μM) and 0.5 mg of TMB were sequentially added to 2 mL citrate buffer solution; (c) 40 μL of H_2O_2 solution (60 μM) was first added to 0.5 mg of $Ce(OH)CO_3$, and reacted at room temperature for 4 min. Subsequently, 2 mL of citrate buffer solution and 0.5 mg of TMB were sequentially added.

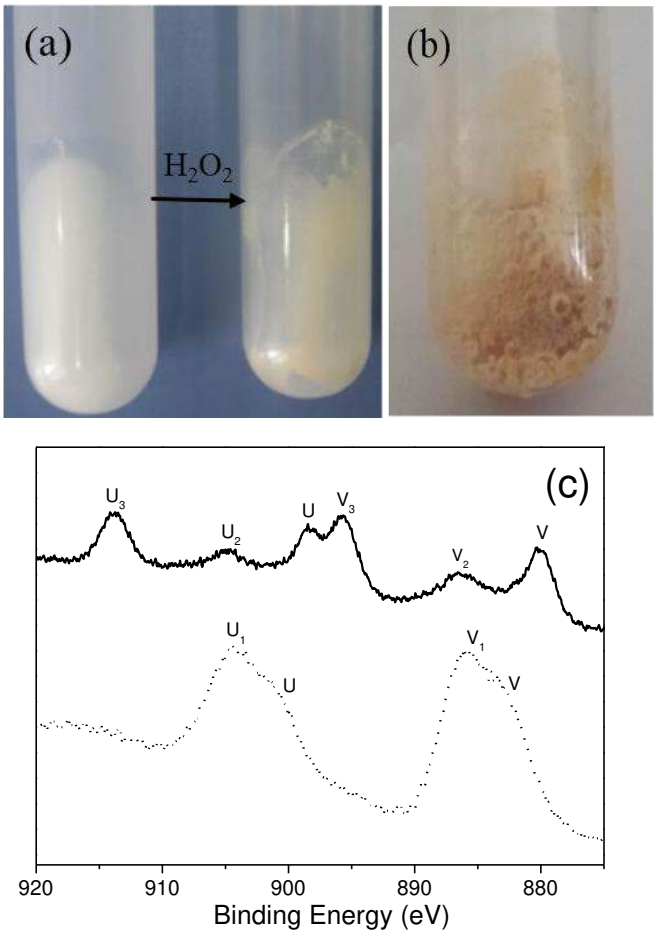

Fig. 3. Upon the addition of H_2O_2, the white color $Ce(OH)CO_3$ powders were changed to the yellow one (a); meanwhile, a number of bubbles appeared in this reaction due to the production of CO_2 and O_2 (b); XPS spectra of Ce 3d for $Ce(OH)CO_3$ before (dotted line) and after (solid line) the reaction with H_2O_2 (c).

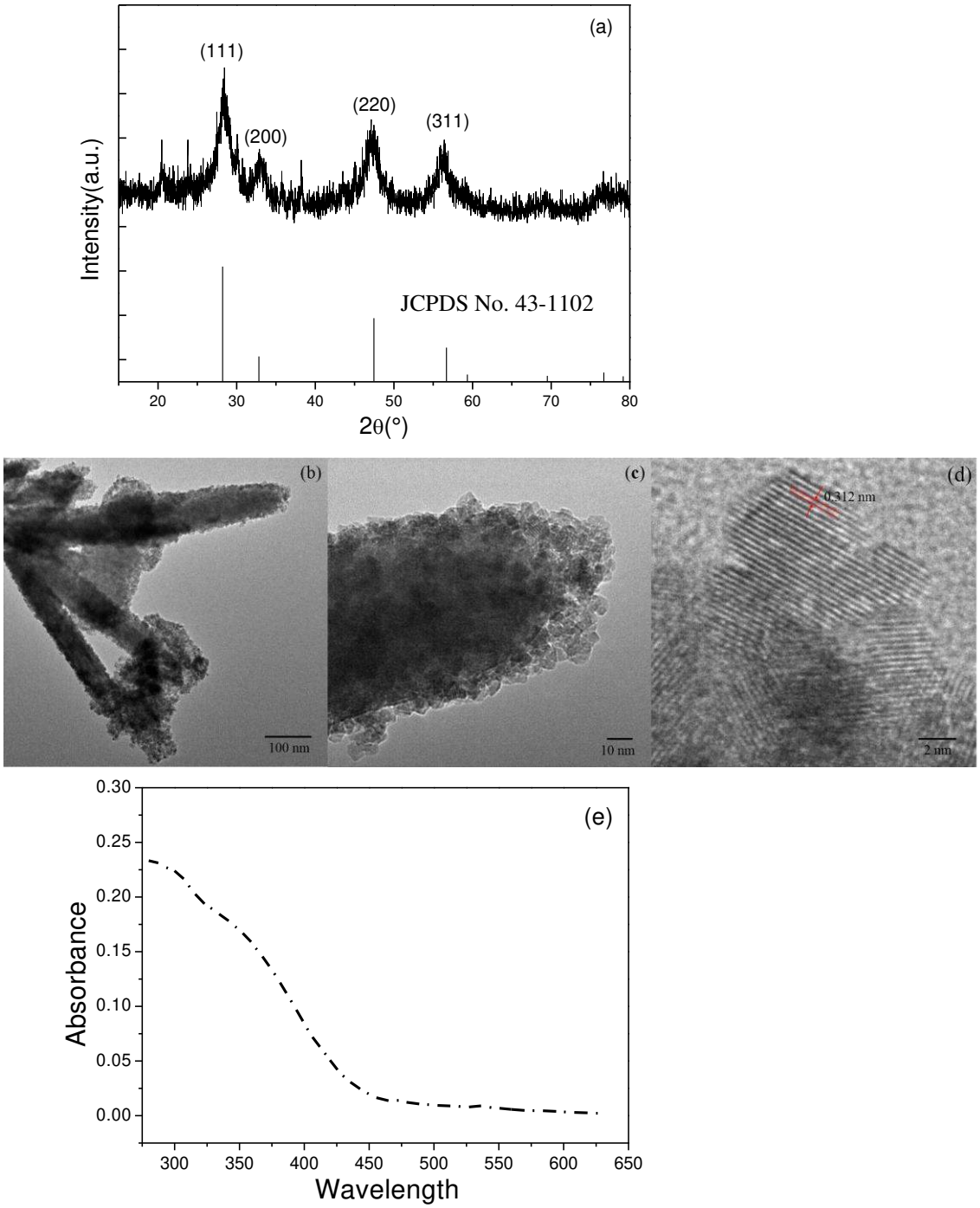

Fig. 4. XRD pattern (a), low (b and c) and high resolution (d) TEM images, and UV-vis absorbance spectrum (e) of the product obtained after the reaction of $Ce(OH)CO_3$ with H_2O_2 at room temperature.

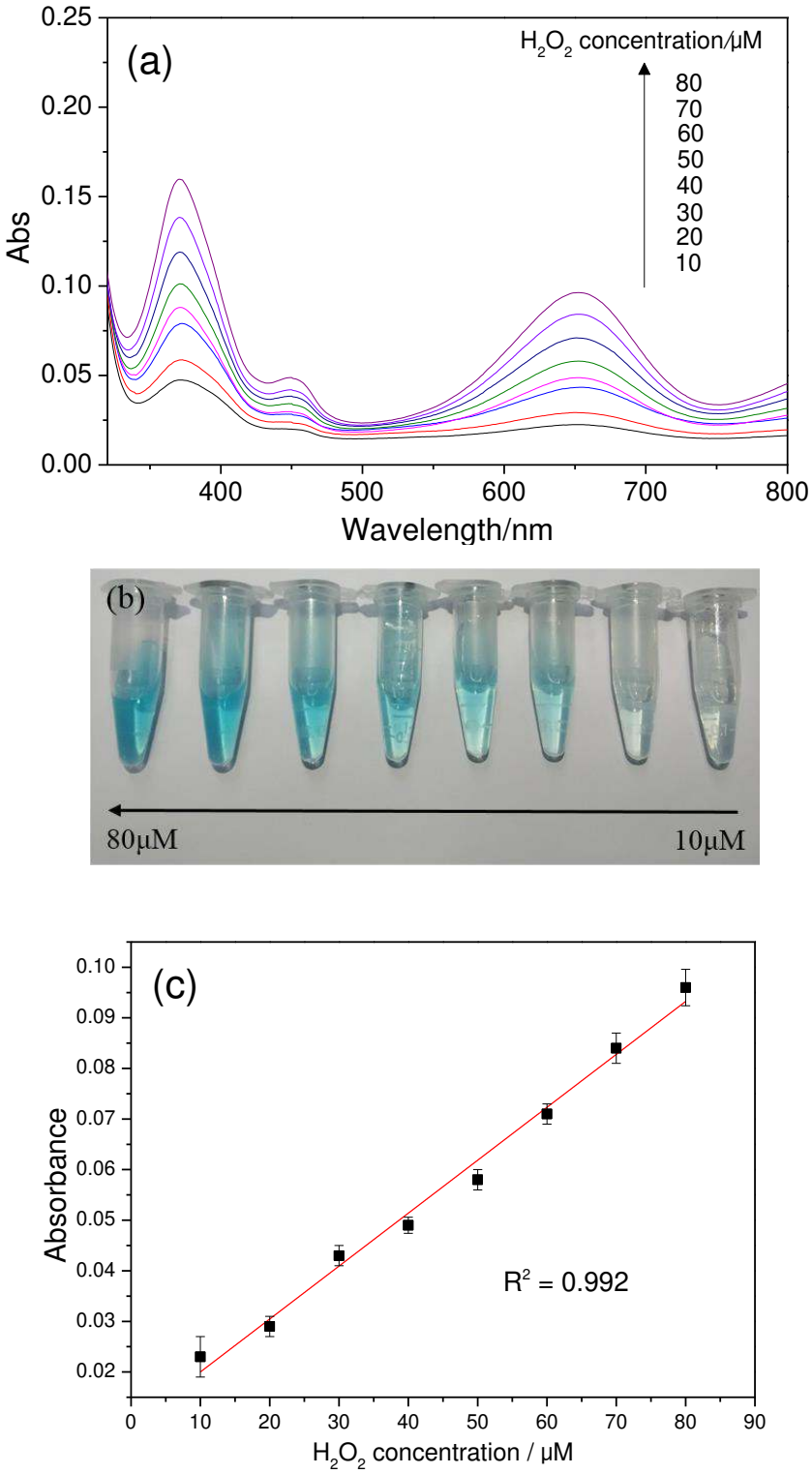

Fig. 5. (a) The UV-vis absorption spectra of the solution after the reaction of $Ce(OH)CO_3$/TMB system with various concentrations of H_2O_2. (b) The corresponding photographs of the reaction solutions with the addition of different concentrations of H_2O_2 ranging from 10 to 80 μM. (b) The absorbance monitored at 652 nm as a function of H_2O_2 concentration.

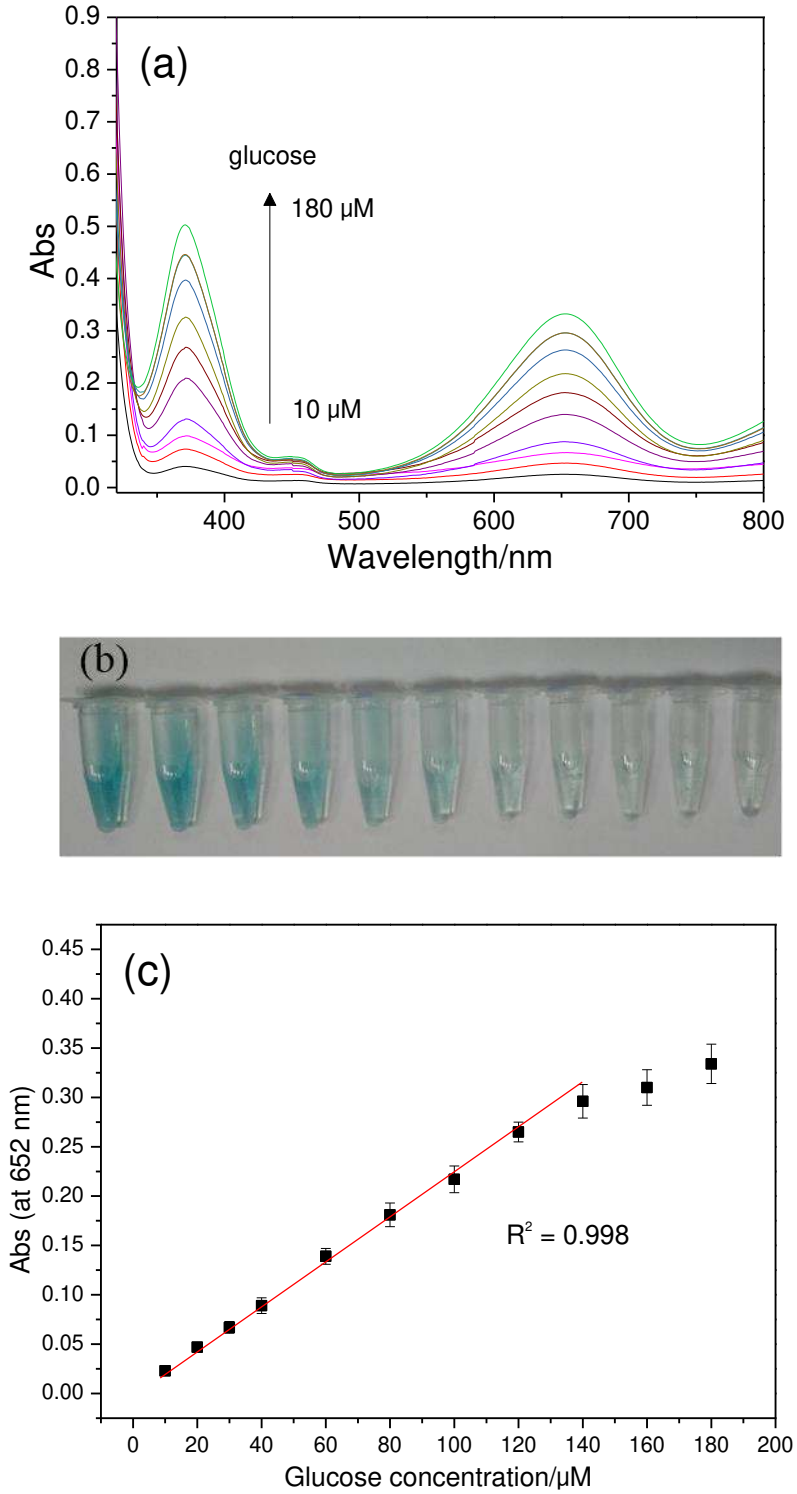

Fig. 6. (a) The UV-vis absorption spectra of the solution after reaction of $Ce(OH)CO_3$/TMB system with various concentrations of glucose in the presence of GOx. (b) The corresponding photographs of the solution after the reaction with the addition of different concentrations of glucose ranging from 10 to 180 μM (from right to left). (c) The absorbance monitored at 652 nm as a function of glucose concentration.

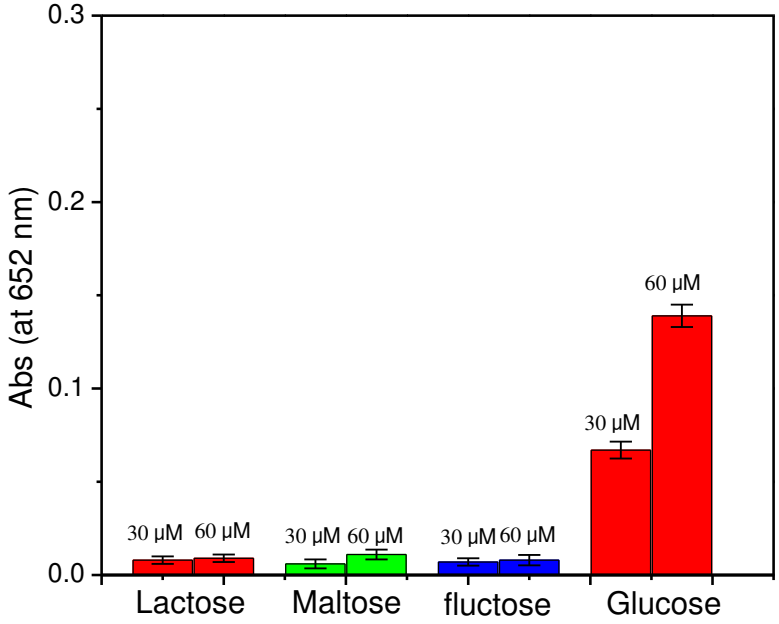

Fig. 7. The absorbance of the solution in the reaction system GOx/$CeOHCO_3$/TMB with the addition of glucose or its analogues such as lactose, fructose and maltose, respectively. The error bars represent the standard deviation obtained by seven repeated experiments.

Table 1. Comparison of the performances of the various types of glucose sensors.

Method	System	Linear range (μM)	LOD (μM)	Reference
Electrochemistry	Pd_1Pt_3-graphene	1 to 23	5	[41]
Electrochemistry	CQDs/octahedral Cu_2O	20 to 4300	8.4	[42]
Electrochemistry	nanoCoPc/Gr	16.7 to 1600	14.6	[43]
Fluorometry	$CePO_4$:Tb colloids/GOx	Up to 120	1.01	[9]
Fluorometry	ZnO/GOx	$1x10^4$ to $1.3x10^5$	$1x10^4$	[12]
Fluorometry	HAQB/GOx	80 to 420	11	[44]
Colorimetry	FeSe/GOx/TMB	2 to 30	0.5	[45]
Colorimetry	Fe_3O_4@C	6 to 100	2	[46]
Colorimetry	Graphene Oxide/ GOx/TMB	1 to 20	1	[47]
Colorimetry	$Ce(OH)CO_3$/GOx/ TMB	up to 140	0.4	This work